JACS
JOURNAL OF THE AMERICAN CHEMICAL SOCIETY

ARTICLE

pubs.acs.org/JACS

Upright Standing Graphene Formation on Substrates

Qinghong Yuan,[†] Hong Hu,[†] Junfeng Gao,[†] Feng Ding,[*,†,§] Zhifeng Liu,[‡] and Boris I. Yakobson[*,†,§,⊥]

[†]Institute of Textiles and Clothing, Hong Kong Polytechnic University, Hong Kong, China

[‡]Department of Chemistry, The Chinese University of Hong Kong, Hong Kong, China

[§]ME&MS Department, Rice University, Houston, Texas 77005, United States

[⊥]Department of Chemistry, Rice University, Houston, Texas 77005, United States

Supporting Information

ABSTRACT: We propose integrating graphene nanoribbons (GNRs) onto a substrate in an upright position whereby they are chemically bound to the substrate at the basal edge. Extensive *ab initio* calculations show that both nickel (Ni)- and diamond-supported upright GNRs are feasible for synthesis and are mechanically robust. Moreover, the substrate-supported GNRs display electronic and magnetic properties nearly the same as those of free-standing GNRs. Due to the extremely small footprint of an upright GNR on a substrate, standing GNRs are ideal building blocks for synthesis of subnanometer electronic or spintronic devices. Theoretically, standing GNR-based microchips with field-effect transistor (FET) densities up to 10^{13} per cm^2 are achievable.

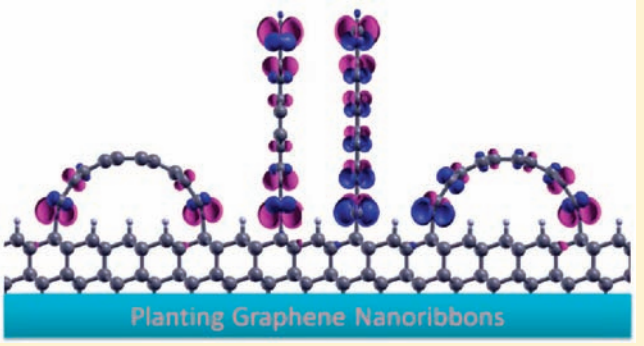

Research on the new star material, graphene, is growing at a speed notably faster than that of its elder sisters [fullerenes (discovered in 1985[1]) and carbon nanotubes (discovered in 1991[2])] due to its intriguing electronic,[3−12] mechanical,[13] chemical[14,15] and thermal properties,[16−18] and numerous potential applications. One of its most promising potential applications is as a future replacement for silicon in electronics and spintronics.[3,5,19−22] For example, the past few years have seen the emergence of an extensive body of literature examining graphene transistors, with a special focus on field-effect transistors (FETs).[23] The motivation for using graphene in electronic devices is to build faster and smaller chips. Given that the commercialized silicon technology of today is capable of producing memory cells with an average half-pitch of 32 nm—which is very close to its quantum limit (i.e., ∼5−10 nm)—graphene-based electronics solutions are being proposed to maintain the famous rule propounded in Moore's Law in the microelectronics of the future. To develop high-performance chips, it is crucial that the average size of the electronic unit (e.g., FET) is reduced and more device units are integrated into each chip.

The application of graphene in FETs requires a medium-sized band gap (e.g., 1.2 eV) and a high carrier mobility. Though pristine graphene has a very high carrier mobility, graphene is a gapless semi-metal.[12] There are several ways to open a medium band gap in graphene for transistor application: (i) introducing defects or doping the graphene;[24,25] (ii) chemical functionalization, e.g. hydrogenation or oxidation;[26−28] and (iii) cutting graphene into one-dimensional (1D) narrow graphene nanoribbons (GNRs).[29−32] Among these methods, (i) and (ii) will significantly reduce carrier mobility by 3−5 orders of magnitude because of the introduction of carrier-scattering centers or charge-trapping sites into the graphene wall.[26,33,34] Although method (iii) may also affect carrier mobility by 1−2 orders of magnitude due to the appearance of edge state, the carrier mobility drop is notably smaller compared with those of (i) and (ii) since only C atoms near the GNR edge are affected.[35,36] Thus, cutting graphene into ribbons is the most desirable method for opening band gaps. Synthesizing high-quality GNRs or cutting graphene into high-quality narrow ribbons presents a big challenge for the fabrication of graphene FETs.[37] High-quality GNRs with well-defined width and edge structures have recently been successfully synthesized by employing a bottom-up method on a transition metal surface.[17] How to integrate these high-quality GNRs into designed devices is also another pressing challenge.

As a two-dimensional (2D) material in a three-dimensional (3D) space, graphene is not mechanically robust to in-plane compression or torque. In practice, free-standing or suspended graphene can be twisted or buckled quite easily.[38−40] This is because the effective thickness of a single layer graphene is very small, $t \approx 0.09$ nm,[41] and thus its flexural rigidity, which is proportional to t^3, is extremely low.[39,42] It is known that any significant mechanical deformation can notably alter the electronic or magnetic properties of GNRs.[12] One can use a substrate to support GNRs to mitigate their mechanical deficiencies. However, when graphene is laid on a substrate, the interaction between

Received: May 4, 2011
Published: September 02, 2011

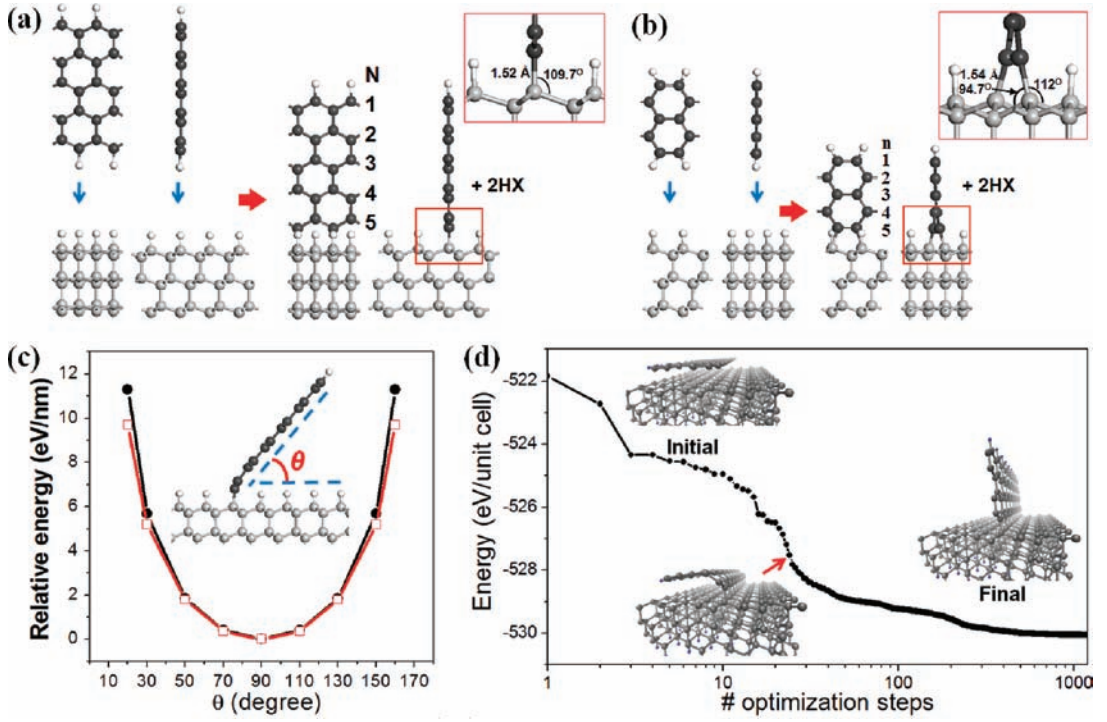

Figure 1. Scheme of X (H or F)-terminated GNRs reacting with a H-passivated diamond (111) surface: (a) and (b) correspond to zigzag- and armchair-edged GNRs, respectively, in which the ribbon widths of the zigzag and armchair GNRs are denoted by *n*. (c) Formation energy of the standing zigzag (black solid circles) and armchair (red open squares) GNRs as a function of the tilted angle, θ. (d) Self-standing up of a GNR initially lying on a diamond (111) surface.

π electrons of this single-atom-thick material and the substrate electrons might significantly change both the electronic structure and the carrier mobility of the graphene. For example, depositing graphene on a SiC surface opens a band gap at the Dirac point.[43] Hence, it will be of both fundamental interest and practical importance to develop methods of integrating GNRs onto substrate without significantly altering their electronic structure or carrier mobility.

In this article, we report a theoretical study of integrating GNR onto a substrate by establishing a strong chemical bond between one edge of the GNR and the substrate. Experimentally, such structures that are called graphene nanowalls (GNWs) in the literature have been synthesized,[44−46] but understanding their formation mechanism and properties is very limited. As examples of two extreme cases, Ni- and diamond-supported standing GNRs (NiSS-GNRs and DSS-GNRs) are thoroughly studied through *ab initio* calculations. Our studies show that both NiSS-GNRs and DSS-GNRs are mechanically robust, and the standing GNRs maintain electronic and magnetic properties very similar to those of free-standing GNRs and ensure a high carrier mobility because most of the π electrons of GNRs are untouched. Beyond these advantages, a standing GNR is only one atom thick, and the distance between standing GNRs on a substrate can be reduced to less than 1 nm. Ideally, the very small distance between standing GNRs opens the door to the fabrication of microchips with an extremely high level of FET density of up to 10^{13} per cm^2, which is about 3−4 orders of magnitude denser than those made using current Si technology.

A DSS-GNR is composed of a diamond substrate, the (111) surface of which is terminated by H atoms, and a standing GNR, in which one of the edges is tightly bound to the diamond surface by strong C−C σ bonds (Figure 1a and b). A NiSS-GNR is constructed by Ni(111) surface and a standing GNR with one edge tightly bound to the nickel surface. For both surfaces, two types of standing GNRs—armchair GNRs (AM-GNRs) and zigzag GNRs (ZZ-GNRs)—are explored. All structures and electronic/magnetic properties are investigated using a density-functional theory (DFT) method implemented in the Vienna ab initio simulation package (VASP). The ion−electron interactions are treated with the projected augmented wave (PAW) pseudopotentials[47,48] using the Perdew−Burke−Ernzerhof (PBE) exchange-correlation functional[49] for the spin-polarized generalized gradient correction. Although the PBE method cannot be used to accurately study the weak interactions, e.g., the interaction between two parallel graphene walls, it is reliable for our study since the upright standing formation of graphene on a substrate is driven by the strong chemical bonding between C atoms on the unpassivated graphene edge and atoms of the substrate. Symmetry-unrestricted optimizations of both geometry and spin are performed using the conjugate gradient scheme until the force component on every atom is less than 0.02 eV/Å, and the energy cutoff chosen is 400 eV. The Brillouin zone is sampled by 28 *k*-points for DSS-GNR and 5 *k*-points for NiSS-GNR along the periodic direction using the Monkhorst−Pack scheme. The diamond (111) surfaces are modeled by six layers of bulk carbon atoms with a vacuum region of more than 10 Å, and the Ni(111) surfaces are modeled by two layers with a fixed bottom layer.

Let us first consider the feasibility of realizing an upright GNR formation on a diamond substrate. Approaching a GNR with free edges (i.e., no edge atom termination) to a bare diamond surface (i.e., no surface passivation) is barrierless and involves a significant

energy deduction. As shown in Supporting Information (SI) Figure S1, our calculation indicates a notable energy deduction of 3.2/4.7 eV per C−C bond for AM/ZZ GNR. There is therefore no doubt that an upright GNR formation can be realized using the chemical operation described above followed by termination/passivation of the GNR/substrate with hydrogen.

It is known that both GNRs with free edges and bare diamond surfaces have high formation energies and thus are not as stable as terminated or passivated ones. Beyond that, the fusion of edge-freed GNRs on a diamond surface may also prevent such a fabrication process. An alternative and more feasible way to synthesize DSS-GNRs is to approach a hydrogen (H)- or fluorine (F)-terminated GNRs to a H-passivated diamond surface and create the standing GNR through recombination of the passivated H and terminated H/F atoms. Figure 1 shows the reaction of an X (X = H or F)-terminated ZZ-GNR (Figure 1a) and AM-GNRs (Figure 1b) with a H-passivated diamond (111) surface. The formation energies (E_F) of the DSS-GNRs are calculated as

$$E_F = E_{DSS\text{-}GNR} + E_{HX} - E_D - E_{GNR}$$

where E_D, E_{GNR}, $E_{DSS\text{-}GNR}$, and E_{HX} are the energies of the diamond substrate, the GNR, the DSS-GNR, and the desorbed HX (i.e., H_2 or HF) molecules, respectively. For X = H, the formation energies of the standing ZZ-GNR and AM-GNR are 0.76 eV/atom and 1.4 eV/atom, respectively, indicating that such a reaction is not energetically preferred. For X = F, the formation energies are significantly reduced to −0.52 eV/atom and 0.04 eV/atom, respectively. Further calculation indicates that the barrier of the reaction between a fluorinated ZZ-GNR and a H-passivated diamond(111) surface is moderate, 2.7 eV (see Figure S2 (SI)). Such a reaction can easily occurr at an elevated temperature, 800−1000 °C, in a few seconds. It can thus be concluded that DSS-GNRs can also be achieved by chemical reactions between terminated GNRs and a passivated diamond surface. The above calculations also indicate that the zigzag DSS-GNRs (DSS-ZZ-GNRs) are energetically more favorable than armchair ones (DSS-AM-GNRs).

The foregoing calculations show that, theoretically, it is possible to realize chemical bonding between GNRs and a substrate by direct assembly of GNRs with a substrate. Experimentally, there's another way to achieve the standing GNR formation: direct growth of upright oriented graphene on a substrate. Very recently, Chen et al. have synthesized vertically oriented graphene on various substrates, from covalent crystal Si to transition metal Au.[44−46] Kondo and co-workers have reported the synthesis of "planar graphene layers standing almost vertically on the substrate".[50] All these present experimental studies showed the potential of synthesizing standing GNR on a properly prepared substrate. Motivated by the recent experimental progress, we have designed an experimental method to achieve the standing GNR pattern with controlled ribbon height (shown in Figure S4 in SI). The synthesis of the standing GNR pattern requires using lithography patterning technology, transition metal catalyzed graphene CVD growth, and ion beam etching technology. Since all these technologies have matured, the success of the GNR pattern synthesis should not a big challenge.

Let us now consider the stability of the standing GNR formation. Structural optimization shows that a GNR standing vertically on the substrate corresponds to a minimum of the potential energy surface (PES) (Figure 1a and b). The energy of the GNR as a function of the tilted angle θ is calculated (Figure 1c) to study the stability of the standing GNR in more detail. It can be seen that $\theta = 90°$ is the global minimum of the PES, demonstrating that GNRs prefer to stand vertically on the substrate surface. For both cases, the energy rises to more than 5.0 eV/nm at $\theta = 30°$, showing the high robusticity of the vertically standing GNR. This can be explained by the strong orientation dependence of the C−C covalent σ bond. For example, for a zigzag GNR, each sp^2 hybridized edge atom on a ZZ-GNR has a dangling bond perpendicularly toward the diamond surface, and each sp^3 hybridized C atom on the diamond surface has another dangling bond in the opposite direction. The meeting of the two unsaturated C atoms forms a strong C−C σ bond perpendicular to the diamond surface (see the inset in Figure 1a). It should be noted that the σ bond is between an sp^2 hybridized C atom (the C atom belongs to the GNR) and an sp^3 hybridized C atom (the C atom belongs to the diamond) and thus carries formation energy of the interface between the GNR and the diamond substrate.[51] However, for the standing AM-GNR, a newly formed C−C bond has to be bent slightly to fit the lattice structure of the diamond (111) surface (inset in Figure 1b). For example, the two bond angles deviate from 109° to 94° and 112°, respectively. This also explains why DSS-ZZ-GNRs are energetically more favorable than DSS-AM-GNRs.

To further demonstrate the robusticity and feasibility of the standing GNR formation, we perform a DFT-based molecular dynamic simulation and a conjugated gradient (CG) optimization in which the initial structure is a zigzag GNR lying flatly on a bare diamond surface. The initial GNR−diamond distance is set as 0.22 nm, significantly larger than the distance of a C−C bond, and the GNR has one H-terminated edge and one unterminated edge. During both the MD simulation and the CG optimization (see SI , ja2037854_si_001.mpg, and ja2037854_si_002.mpg for details), with a notable energy deduction, the chemical bonds between the unterminated GNR edge and the bare diamond surface form quickly (Figure 1d). Formation of the chemical bonds initially results in a high degree of curvature in the ribbon wall (see insets in Figure 1d). The GNR then stands up slowly with an energy reduction due to relaxation of its curvature energy.

It is not a surprise that a chemically bonded GNR tends to stand vertically on a diamond surface because of the strong orientation dependence of the C−C covalent bind at the GNR−diamond interface. The similar standing GNR formation can be expected to be achieved on other substrate materials such as Si, SiO_2, Al_2O_3, or SiC. To further illustrate the universality of the standing GNR formation on a flat substrate, the standing GNR formation on a typical transition metal surface, Ni (111), is shown in Figure 2. For a GNR which interacts with the Ni(111) surface through a free edge, the upright position, where the tilt angle $\theta = 90°$, is the global minimum of the potential energy surface. However, the small energy change indicates that its tendency of standing up is weaker than that on a diamond surface. The energy change from the global minimum, $\theta = 90°$, to $\theta = 30°$ is about 2.5 eV, which is about half the corresponding energy change on a diamond surface, ∼5.0 eV.

In addition to the feasibility and robusticity of DSS-GNRs, their electronic and magnetic properties are also attractive. Several previous studies have indicated that graphene−substrate interaction may greatly change the electronic and magnetic properties of pristine graphene.[43,52] In this context, only one edge of the standing GNR interacts with the substrate. The π electrons in most parts of the GNR, especially those around its

upper edge, therefore remain untouched. Thus, we can anticipate a uniform electronic structure along the supported 1D GNR and consequently a high carrier mobility in the standing GNR. According to the well-established tight binding (TB) model, the confinement of π electrons along the width direction of a GNR fully determines the GNR's electronic structure.[53−56] One edge of a GNR standing on a diamond surface is terminated by H atoms, while another edge is terminated by the diamond, which is a wide band gap semiconductor. The π electrons of the GNR should therefore be well-confined between the H-terminated edge and the substrate. We thus anticipate that each DSS-GNR has an electronic structure similar to that of the corresponding free-standing GNR. To test this prediction, a series of calculations are carried out to explore the electronic and magnetic properties of DSS-GNRs.

We first explore DSS-AM-GNR(n) in which the width n varies from 1 to 12. Our calculations demonstrate that in common with free-standing AM-GNRs,[53,57] the ground state of DSS-AM-GNR(n) is nonmagnetic. In addition, the band gaps of DSS-AM-GNR(n) exhibit a width-dependent oscillation (Figure 3a) with a periodicity of 3, following a hierarchy of $\Delta_{3p+2} < \Delta_{3p+1} < \Delta_{3p}$ where p is a positive integer. This hierarchy is different from that of free-standing AM-GNRs where $\Delta_{3p+2} < \Delta_{3p} < \Delta_{3p+1}$.[53,57] This difference apparently originates from the unique edge termination of standing GNRs: both edges of a free-standing AM-GNR are terminated by H atoms, while one edge of a standing GNR is terminated by the diamond substrate. As an example, graphs b, c, and d of Figure 3 show the band structure and density of states (DOS) of DSS-AM-GNR(n) with n = 10, 11, and 12, respectively, together with the band-decomposed charge densities of the valence band maximum (VBM) and the conducting band minimum (CBM). It can be seen that both the valence band and the conducting band originate from the constituent ribbon. Among the three ribbons, the DSS-AM-GNR(11) has the smallest band gap, and we can see that the charge of the VBM or CBM is localized in the constituent ribbon only. This is because both the VBM and CBM energies are located within the diamond band gap, and thus there is no band mixture between the GNR and the diamond substrate, while a noticeable band mixture of VBM in DSS-AM-GNR(n = 12) is also observed (Figure 3d). One can see that the valence band of the GNR meets that of the diamond substrate, leading to a mixture of the two bands. As a consequence, the charge distribution of the VBM for n = 12 disperses from the ribbon side into the diamond substrate (graphic A in Figure 3d).

Although their band gap hierarchy is different from that of free-standing AM-GNRs, the electronic structure of the DSS-AM-GNRs around the Fermi level, e.g., the size of the band gap opening as a function of ribbon width and the dispersion of orbitals in the ribbon,[53,57] is almost the same. We therefore conclude that DSS-AM-GNRs retain the electronic properties of corresponding free-standing AM-GNRs. This result is in good agreement with the prediction of the TB model in which only the ribbon width is a dominating parameter.

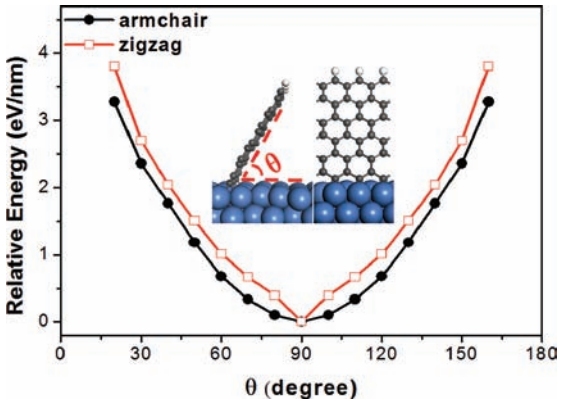

Figure 2. Upright standing graphene nanoribbon formation on Ni-(111) surface (inset) and the corresponding relative energy as a function of the tilt angle.

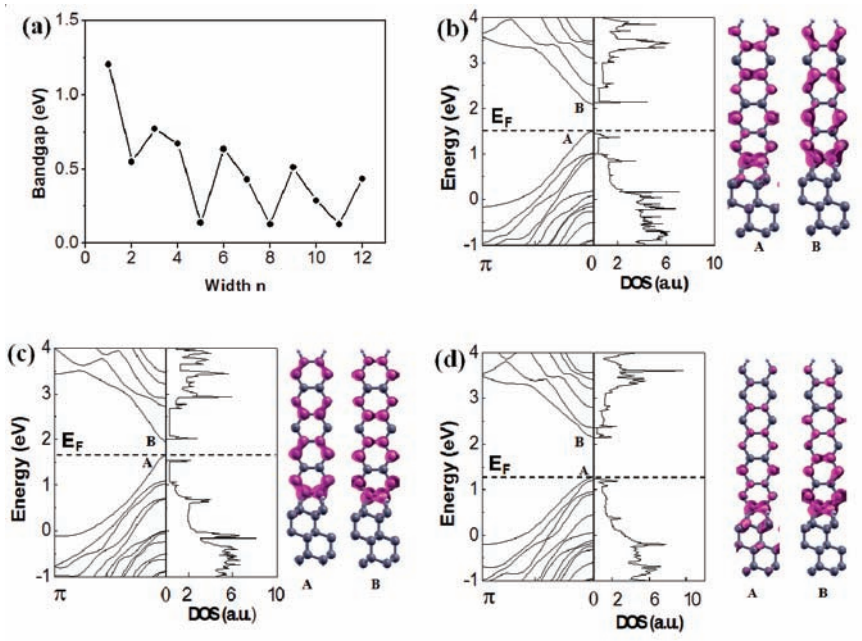

Figure 3. (a) Band gap of the DSS-AM-GNRs as a function of width n. Band structure, density of states (DOS), and band-decomposed charge densities of VBM and CBM at the gamma point (Γ) for (b) n = 10, (c) n = 11, and (d) n = 12.

dx.doi.org/10.1021/ja2037854 |J. Am. Chem. Soc. 2011, 133, 16072–16079

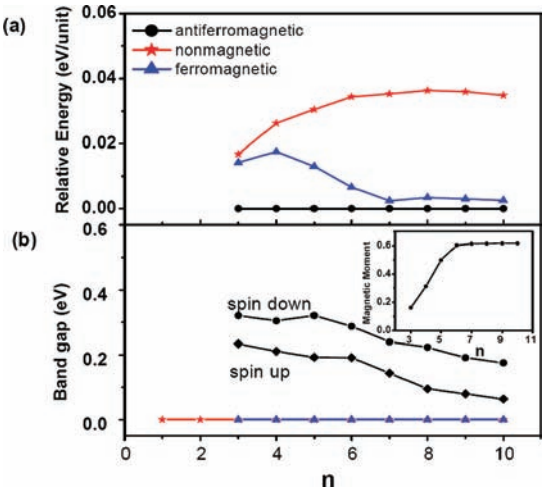

Figure 4. (a) Relative energies of the DSS-ZZ-GNRs as a function of ribbon width n for antiferromagnetic (AFM), ferromagnetic (FM), and nonmagnetic (NM) states. (b) Band gap of the DDS-ZZ-GNR(n) as a function of ribbon width n for AFM, FM, and NM states. Inset in (b) shows the magnetic moment (in units of μm) of the FM state as a function of ribbon width n.

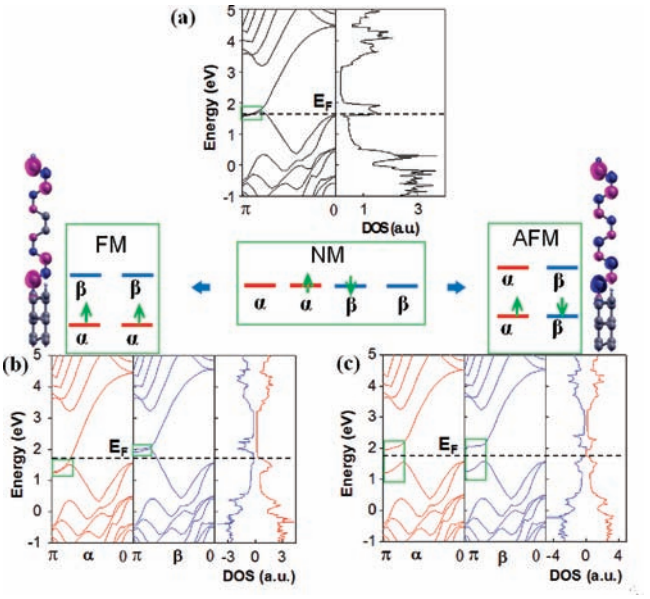

Figure 5. Band gap and density of states (DOS) near the Fermi level for (a) nonmagnetic (NM), (b) ferromagnetic (FM), and (c) antiferromagnetic (AFM) states of DSS-ZZ-GNR($n = 6$). The magnetic moment distributions (red represents spin up density and blue represents spin down density) for the FM and AFM states are also inserted in (b) and (c).

Free-standing ZZ-GNRs are distinguished by their magnetic property. A free-standing ZZ-GNR has an antiferromagnetic ground state in which its two edges have opposite magnetic moments. The ground state is semiconducting with a narrow band gap.[53,58,59] A strong transverse electric field can turn a ZZ-GNR into a half-metal, thus enabling ZZ-GNRs to be used as building blocks for spintronic devices.[19−22]

As shown in Figure 4a, the ground states of extremely narrow DSS-ZZ-GNRs (n = 1, 2) are nonmagnetic, and the magnetic (either ferromagnetic or antiferromagnetic, respectively) states are unstable, which is different from those of H-passivated GNRs.[22] The difference can be attributed to the very different edge termination. For $n > 3$, a more general pattern of behavior emerges whereby the nonmagnetic (NM) state is less stable than the magnetic one, but all states have very close energies. The energy of the NM state is slightly higher than that of the ferromagnetic (FM) and antiferromagnetic (AFM) state (the energy difference is ∼0.03−0.04 eV/unit cell). Although the AFM state is always the ground state for $n > 3$, the energy difference between the FM and AFM states becomes negligible (only ∼0.01 eV/unit cell) for $n > 6$. A similar trend has been reported for free-standing ZZ-GNRs.[58,59] Both the NM and FM states are conductive, while the AFM state has a small band gap that varies between 0.1 and 0.4 eV (Figure 4b). It should be noted that the DFT method might notably underestimate the band gap of the ribbon. With reasonable correction, the band gap of the AFM state might be as high as 1.0 eV.[53] The magnetic moment of the metastable FM state increases monotonically with ribbon width n and approaches a saturated value of 0.6 μm per unit cell (the number would be 0.49 μm per unit cell if the PW91 functional was used) (see the inset in Figure 4b).

To gain deep insight into the origins of the three DSS-ZZ-GNR states, we take $n = 6$ as an example to calculate their band structures, DOS, and the band-decomposed charge densities of bands near the Fermi level. As shown in Figure 5a, the valence band (VB) and conducting band (CB) of the NM state are nearly degenerated in the region $k \in [3/4\pi, \pi]$. Only half of the VB and CB are therefore occupied in this region. Taking spin polarization into account, four nearly degenerated bands (or orbitals) can be identified in the $[3/4\pi, \pi]$ region: two spin up (α) bands and two spin down (β) bands. Because these four bands are only half occupied (Figure 5a), they are metastable and tend to split into two lower-energy occupied bands and two higher-energy unoccupied bands with a reduction in total energy. There are two ways in which these four bands split: (i) Figure 5a → Figure 5b in which bands with different spins split and both occupied lower-energy bands are α bands, which correspond to the FM state; (ii) Figure 5a → Figure 5c in which bands with the same spin (α or β) split and result in one occupied α band and one occupied β band. Given that the α band and the β band are equally occupied, the total magnetic moment of the system remains zero; this corresponds to the AFM state. For the FM state, because the two occupied α bands (which can be regarded as CB and VB) intersect each other in the $[3/4\pi, \pi]$ region, it is conductive (Figure 5b); for the AFM state, the splitting up of the α and β bands leads to a band gap (Figure 5c) and thus enhances the stability of the system.

The foregoing analysis explains the energy order of the NM, FM, and AFM states and their corresponding electronic and magnetic properties. Together with the band-decomposed charge densities of bands near the Fermi surface (see SI, Figure S3), one can see that termination of the GNR edge by the diamond surface has only a minor effect on the electronic and magnetic properties of the GNRs.

In sum, our calculations show that standing GNRs have electronic and magnetic properties very similar to those of corresponding free-standing GNRs. Although the dispersion of orbitals into the substrate might result in a slight change to the electronic structure of a standing GNR, the overall electronic/magnetic properties of the standing ribbon are quite robust, indicating that diamond passivation has only a small impact on

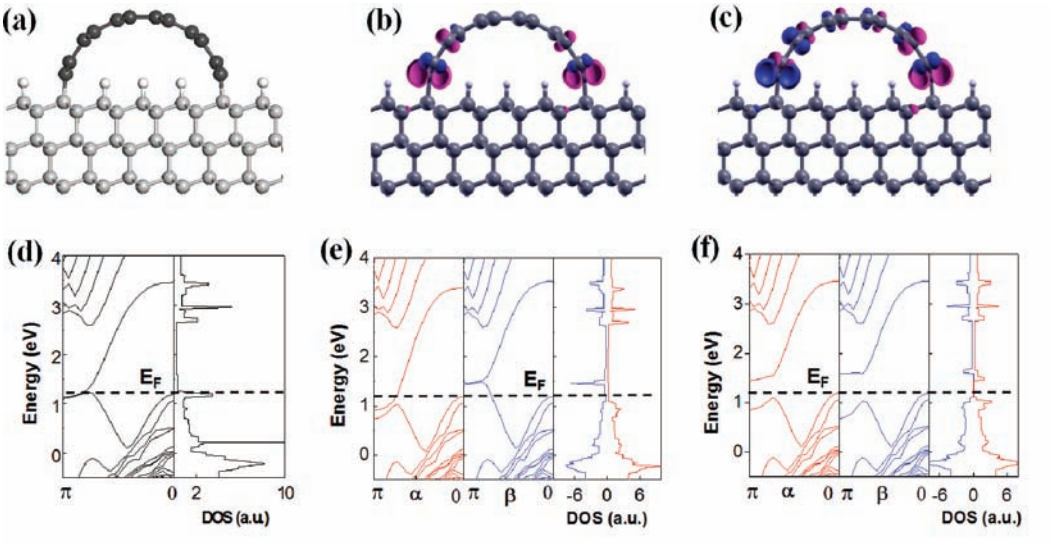

Figure 6. (a) Partial SWNT (p-SWNT) formation of a ZZ-GNR(6) with both edges bound to a diamond (111) surface. Magnetic moment distributions of its ferromagnetic (b) and antiferromagnetic (c) states. Band gap and density of states (DOS) for nonmagnetic (d), ferromagnetic (e), and antiferromagnetic (e) states of the GNR.

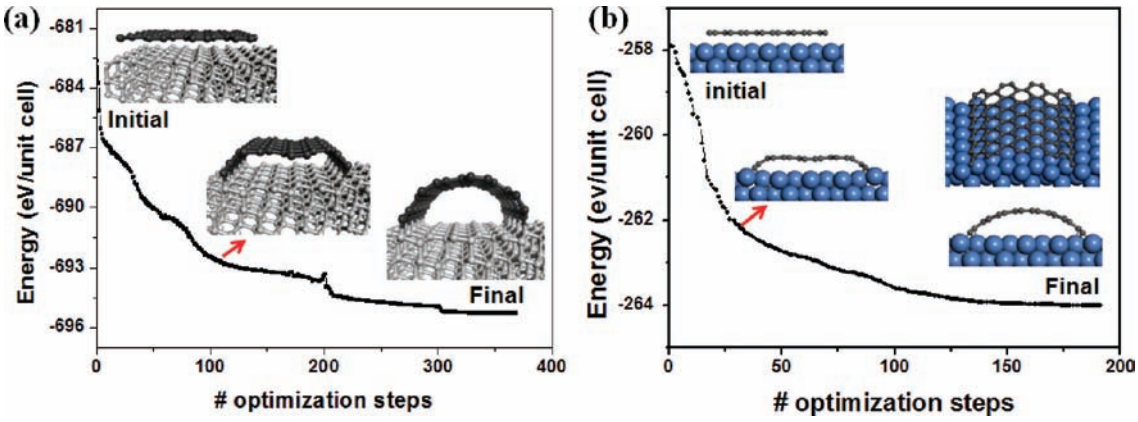

Figure 7. Formation of partial single walled carbon nanotubes (p-SWNT) on (a) diamond (111) surface and on Ni(111) surface and the total energy change during the conjugated gradient structural optimization.

the electronic structure of GNRs in comparison with the impacts on ribbon width and orientation.

The robusticity of the electronic/magnetic properties of GNRs can also be seen in another type of supported GNR in which both edges of the ribbon are chemically bound to the substrate (Figure 6). This newly designed GNR on a substrate surface has a considerable bend in its graphene wall and resembles a partial single-walled carbon nanotube (p-SWNT). Formation of a p-SWNT on a substrate further enhances the flexural rigidity of the GNR because both edges are tightly bound to the substrate, and its effective thickness is therefore enhanced. It is interesting to note that in a manner similar to that of standing GNRs, the electronic and magnetic properties of a p-SWNT remain the same as those of a corresponding free-standing GNR. Zigzag-edged p-SWNTs have been identified as having three electronic states—the NM, FM, and AFM states—and their ground state is again AFM. The band structures and DOS of the three states are shown in Figure 6d, e, and f, respectively. Compared with those shown in Figure 5, we can see that there is almost no change in their electronic and magnetic properties. In terms of the magnetic moment distributions of the FM and AFM states (Figure6b and c), the p-SWNT shown in Figure 6 closely resembles a bent DSS-ZZ-GNR(6).

Though the electronic and magnetic properties of the p-SWNT are not significantly altered, the p-SWNT surface has a large curvature, and the distributions of π electrons outside and inside the p-SWNT wall are asymmetric. It can be seen that the magnetic moment distribution outside the p-SWNT wall is more abundant than that inside the wall. Its large curvature must also affect its chemical properties as in SWNTs and fullerenes.[60,61] For example, the wall of the p-SWNT can be more easily functionalized from outside than flat graphene or GNRs.[61]

Similar to the standing GNR formation, the p-SWNT on diamond surface can be simply realized by placing a free ended GNR onto an unpassivated diamond surface. As shown in Figure 7a (for details see ja2037854_si_004.avi and ja2037854_si_005.avi in SI), C atoms on both free edges of the GNR forming strong C−C covalent bonds with C atoms of the diamond surface lead

to a significant energy drop in the initial stage of the conjugated gradient (CG) structure optimization. Then the tendency of both GNR edges standing up lifts the flat wall of GNR to form a p-SWNT on the diamond surface. One might argue that the merging of two unterminated edges of a GNR prefers a stable SWNT formation than a p-SWNT. It should be noted that there is a large barrier that prevents the SWNT formation because of the rising of its curvature energy and edge formation energy.

A very similar process can be seen in the CG optimization of free-edged GNRs on the Ni (111) surface (Figure 7b and movies ja2037854_si_004.avi and ja2037854_si_005.avi in SI). The tendency of standing up first changes the wall orientation near both GNR edges while the central part remains flat with a significant energy drop. Then it gradually turns the GNR wall into a p-SWNT. While, as a consequence of stronger binding between GNR edge and diamond surface, the p-SWNT on diamond surface has significantly larger curvature than that on a Ni(111) surface (Figure 7). Roughly, the GNR was turned into a 1/4-SWNT on the Ni(111) and a 2/5-SWNT on the diamond (111) surface, respectively.

In conclusion, we propose a method of integrating graphene nanoribbons (GNRs) onto substrates with significantly enhanced flexural rigidity while retaining the electronic and magnetic properties and high carrier mobility of pristine GNRs. We study in detail both Ni- and diamond-supported standing GNRs (DSS-GNRs) and partial SWNTs (in which both edges of the ribbons are tightly bound to the Ni or diamond substrate) as examples. The results show that both standing GNRs and p-SWNTs maintain the electronic and magnetic properties of pristine GNRs. Not only does this new method maintain the uniform structure of the standing ribbons or p-SWNTs, which ensures they have carrier mobility as high as that of pristine GNRs, this method of integrating GNRs onto a substrate also opens the door to the synthesis of high-performance graphene-based electronic and magnetic devices such as FETs with a high on/off current ratio. In comparison with GNRs laid on a substrate, standing GNRs have an extremely narrow footprint/projected width on the substrate (i.e., one atom thick), and their electronic properties can be tuned by changing their height. To maintain the independent electronic properties of neighboring GNRs, it may be necessary to space them at a distance of 0.7−1.0 nm, which is double or triple the layer−layer distance in graphite. The new technology discussed in this paper therefore lays the groundwork for the development of subnanometer electronic technology. Supposing an area of 10 nm^2 is required to build a device unit on a chip, such technology may make it possible to produce high-performance electronic chips with an extremely high unit density of $10^{13}/cm^2$.

■ ASSOCIATED CONTENT

Ⓢ Supporting Information. A molecular dynamic simulation (ja2037854_si_001.mpg) and a conjugated gradient optimization (ja2037854_si_002.mpg) of a GNR initially lying flat before standing up on a bare diamond (111) surface; CG optimization of the partial-SWNT formation on a diamond (111) surface (ja2037854_si_003.avi) and on a Ni(111) surface (ja2037854_si_004.avi and ja2037854_si_005.avi); a scheme for free-edged GNRs reacting with a bare diamond (111) surface (Figure S1); potential energy surface of a fluorinated zigzag GNR reacting with a hydrogenated diamond (111) surface (Figure S2); the band structure and band-decomposed charge densities of VBM and CBM for DSS-ZZ-GNR(6) (Figure S3); and an illustration of an experimental method of synthesizing the standing GNR pattern with controlled height (Figure S4). This material is available free of charge via the Internet at http://pubs.acs.org.

■ AUTHOR INFORMATION

Corresponding Author
tcfding@inet.polyu.edu.hk; biy@rice.edu

■ ACKNOWLEDGMENT

Work at Rice was supported by the National Science Foundation (CBET) and partially by the Air Force Office of Scientific Research (MURI). B.I.Y. acknowledges the Royal Society (London) Visiting Professorship award which enabled this collaboration. Work done at PolyU was supported by Hong Kong Polytechnic University projects (A-PJ50, A-PH93, A-PD1U) and the National Natural Science Foundation of China grants (10725418, 10734090, 10990104). Computational resource allocation from the Shanghai Supercomputer Center is also acknowledged.

■ REFERENCES

(1) Kroto, H. W.; Heath, J. R.; O'Brien, S. C.; Crul, R. F.; Smalley, R. E. *Nature* **1985**, *318*, 162–163.
(2) Iijima, S. *Nature* **1991**, *354*, 56–58.
(3) Novoselov, K. S.; Geim, A. K.; Morozov, S. V.; Jiang, D.; Zhang, Y.; Dubonos, S. V.; Grigorieva, I. V.; Firsov, A. A. *Science* **2004**, *306*, 666–669.
(4) Gusynin, V. P.; Sharapov, S. G. *Phys. Rev. Lett.* **2005**, *95*, 146801/1–146801/4.
(5) Novoselov, K. S.; Jiang, Z.; Zhang, Y.; Morozov, S. V.; Stormer, H. L.; Zeitler, U.; Maan, J. C.; Boebinger, G. S.; Kim, P.; Geim, A. K. *Science* **2007**, *315*, 1379–1379.
(6) Peres, N. M. R.; Guinea, F.; Neto, A. H. C. *Phys. Rev. B* **2006**, *73*, 125411/1–125411/23.
(7) Zhang, Y. B.; Tan, Y. W.; Stormer, H. L.; Kim, P. *Nature* **2005**, *438*, 201–204.
(8) Latil, S.; Henrard, L. *Phys. Rev. Lett.* **2006**, *97*, 036803/1–036803/4.
(9) Nair, R. R.; Blake, P.; Grigorenko, A. N.; Novoselov, K. S.; Booth, T. J.; Stauber, T.; Peres, N. M. R.; Geim, A. K. *Science* **2008**, *320*, 1308–1308.
(10) Eda, G.; Fanchini, G.; Chhowalla, M. *Nat. Nanotechnol.* **2008**, *3*, 270–274.
(11) Kuzmenko, A. B.; van Heumen, E.; Carbone, F.; van der Marel, D. *Phys. Rev. Lett.* **2008**, *100*, 117401/1–11740/4.
(12) Castro Neto, A. H.; Guinea, F.; Peres, N. M. R.; Novoselov, K. S.; Geim, A. K. *Rev. Mod. Phys.* **2009**, *81*, 109–162.
(13) Lee, C.; Wei, X. D.; Kysar, J. W.; Hone, J. *Science* **2008**, *321*, 385–388.
(14) Choi, J.; Kim, K. J.; Kim, B.; Lee, H.; Kim, S. *J. Phys. Chem. C* **2009**, *113*, 9433–9435.
(15) Hamilton, C. E.; Lomeda, J. R.; Sun, Z. Z.; Tour, J. M.; Barron, A. R. *Nano Lett.* **2009**, *9*, 3460–3462.
(16) Seol, J. H.; Jo, I.; Moore, A. L.; Lindsay, L.; Aitken, Z. H.; Pettes, M. T.; Li, X. S.; Yao, Z.; Huang, R.; Broido, D.; Mingo, N.; Ruoff, R. S.; Shi, L. *Science* **2010**, *328*, 213–216.
(17) Cai, W.; Moore, A. L.; Zhu, Y.; Li, X.; Chen, S.; Shi, L.; Ruoff, R. S. *Nano Lett.* **2010**, *10*, 1645–1651.
(18) Munoz, E.; Lu, J.; Yakobson, B. I. *Nano Lett.* **2010**, *10*, 1652–1656.
(19) Hod, O.; Barone, V.; Peralta, J. E.; Scuseria, G. E. *Nano Lett.* **2007**, *7*, 2295–2299.
(20) Kan, E. J.; Li, Z. Y.; Yang, J. L.; Hou, J. G. *Appl. Phys. Lett.* **2007**, *91*, 243116.

(21) Hod, O.; Barone, V.; Scuseria, G. E. *Phys. Rev. B* **2008**, *77*, 035411/1–035411/6.
(22) Son, Y. W.; Cohen, M. L.; Louie, S. G. *Nature* **2006**, *444*, 347–349.
(23) Schwierz, F. *Nat. Nanotechnol.* **2010**, *5*, 487–496.
(24) Ci, L.; Song, L.; Jin, C. H.; Jariwala, D.; Wu, D. X.; Li, Y. J.; Srivastava, A.; Wang, Z. F.; Storr, K.; Balicas, L.; Liu, F.; Ajayan, P. M. *Nat. Mater.* **2010**, *9*, 430–435.
(25) Zanella, I.; Guerini, S.; Fagan, S. B.; Mendes, J.; Souza, A. G. *Phys. Rev. B* **2008**, *77*, 073404/1–073404/4.
(26) Elias, D. C.; Nair, R. R.; Mohiuddin, T. M. G.; Morozov, S. V.; Blake, P.; Halsall, M. P.; Ferrari, A. C.; Boukhvalov, D. W.; Katsnelson, M. I.; Geim, A. K.; Novoselov, K. S. *Science* **2009**, *323*, 610–613.
(27) Yan, J. A.; Xian, L. D.; Chou, M. Y. *Phys. Rev. Lett.* **2009**, *103*, 086802/1–086802/4.
(28) Gilje, S.; Han, S.; Wang, M.; Wang, K. L.; Kaner, R. B. *Nano Lett.* **2007**, *7*, 3394–3398.
(29) Han, M. Y.; Ozyilmaz, B.; Zhang, Y. B.; Kim, P. *Phys. Rev. Lett.* **2007**, *98*, 206805/1–206805/4.
(30) Berger, C.; Song, Z. M.; Li, X. B.; Wu, X. S.; Brown, N.; Naud, C.; Mayou, D.; Li, T. B.; Hass, J.; Marchenkov, A. N.; Conrad, E. H.; First, P. N.; de Heer, W. A. *Science* **2006**, *312*, 1191–1196.
(31) Ci, L.; Xu, Z. P.; Wang, L. L.; Gao, W.; Ding, F.; Kelly, K. F.; Yakobson, B. I.; Ajayan, P. M. *Nano Res.* **2008**, *1*, 116–122.
(32) Chen, Z. H.; Lin, Y. M.; Rooks, M. J.; Avouris, P. *Physica E* **2007**, *40*, 228–232.
(33) Wang, S.; Ang, P. K.; Wang, Z. Q.; Tang, A. L. L.; Thong, J. T. L.; Loh, K. P. *Nano Lett. 10*, 92-98.
(34) Su, C. Y.; Xu, Y. P.; Zhang, W. J.; Zhao, J. W.; Liu, A. P.; Tang, X. H.; Tsai, C. H.; Huang, Y. Z.; Li, L. J. *ACS Nano 4*, 5285-5292.
(35) Betti, A.; Fiori, G.; Iannaccone, G.; Mao, Y. IEEE. In *2009 IEEE International Electron Devices Society Meeting*; IEEE: New York, 2009; pp 837−840.
(36) Li, X. L.; Wang, X. R.; Zhang, L.; Lee, S. W.; Dai, H. J. *Science* **2008**, *319*, 1229–1232.
(37) Jiao, L. Y.; Wang, X. R.; Diankov, G.; Wang, H. L.; Dai, H. J. *Nat. Nanotechnol.* **2010**, *5*, 321–325.
(38) Shenoy, V. B.; Reddy, C. D.; Ramasubramaniam, A.; Zhang, Y. W. *Phys. Rev. Lett.* **2008**, *101*, 245501/1–245501/4.
(39) Bets, K. V.; Yakobson, B. I. *Nano Res.* **2009**, *2*, 161–166.
(40) Meyer, J. C.; Geim, A. K.; Katsnelson, M. I.; Novoselov, K. S.; Booth, T. J.; Roth, S. *Nature* **2007**, *446*, 60–63.
(41) Kudin, K. N.; Scuseria, G. E.; Yakobson, B. I. *Phys. Rev. B* **2001**, *64*, 235406/1–235406/10.
(42) Zhu, L.; Wang, J.; Zhang, T.; Ma, L.; Lim, C. W.; Ding, F.; Zeng, X. C. *Nano Lett.* **2010**, *10*, 494–498.
(43) Zhou, S. Y.; Gweon, G. H.; Fedorov, A. V.; First, P. N.; De Heer, W. A.; Lee, D. H.; Guinea, F.; Neto, A. H. C.; Lanzara, A. *Nat. Mater.* **2007**, *6*, 770–775.
(44) Bo, Z.; Yu, K.; Lu, G.; Wang, P.; Mao, S.; Chen, J. *Carbon* **2011**, *49*, 1849.
(45) Yu, K.; Bo, Z.; Lu, G.; Mao, S.; Cui, S.; Zhu, Y.; Chen, X.; Ruoff, R. S.; Chen, J. *Nanoscale Res. Lett.* **2011**, *6* (6), 202, DOI: , 10.1186/1556-276X-6-202.
(46) Yu, K.; Wang, P.; Lu, G.; Chen, K. H.; Bo, Z.; Chen, J. *J. Phys. Chem. Lett.* **2011**, *2*, 537.
(47) Blochl, P. E. *Phys. Rev. B* **1994**, *50*, 17953–17979.
(48) Kresse, G.; Joubert, D. *Phys. Rev. B* **1999**, *59*, 1758–1775.
(49) Perdew, J. P.; Burke, K.; Ernzerhof, M. *Phys. Rev. Lett.* **1996**, *77*, 3865–3868.
(50) Kondo, S.; Kawai, S.; Takeuchi, W.; Yamakawa, K.; Den, S.; Kano, H.; Hiramatsu, M.; Hori, M. *J. Appl. Phys.* **2009**, *106*, 094302.
(51) Lin, Y.; Ding, F.; Yakobson, B. I. *Phys. Rev. B* **2008**, *78*, 041402/1–041402/4.
(52) Giovannetti, G.; Khomyakov, P. A.; Brocks, G.; Kelly, P. J.; van den Brink, J. *Phys. Rev. B* **2007**, *76*, 073103/1–073103/4.
(53) Son, Y. W.; Cohen, M. L.; Louie, S. G. *Phys. Rev. Lett.* **2006**, *97*, 216803/1–216803/4.
(54) Yang, L.; Park, C. H.; Son, Y. W.; Cohen, M. L.; Louie, S. G. *Phys. Rev. Lett.* **2007**, *99*, 186801/1–186801/4.
(55) Akhmerov, A. R.; Beenakker, C. W. J. *Phys. Rev. B* **2008**, *77*, 085423/1–085423/10.
(56) Brey, L.; Fertig, H. A. *Phys. Rev. B* **2006**, *73*, 235411/1–235411/5.
(57) Barone, V.; Hod, O.; Scuseria, G. E. *Nano Lett.* **2006**, *6*, 2748–2754.
(58) Pisani, L.; Chan, J. A.; Montanari, B.; Harrison, N. M. *Phys. Rev. B* **2007**, *75*, 064418/1–064418/9.
(59) Kudin, K. N. *ACS Nano* **2008**, *2*, 516–522.
(60) Lu, X.; Chen, Z. F. *Chem. Rev.* **2005**, *105*, 3643–3696.
(61) Zheng, G. S.; Wang, Z.; Irle, S.; Morokuma, K. *J. Am. Chem. Soc.* **2006**, *128*, 15117–15126.